Nanoscale

RSC Publishing

PAPER

View Article Online
View Journal | View Issue

Cite this: *Nanoscale*, 2013, **5**, 780

Comparison of electrochemical performances of olivine $NaFePO_4$ in sodium-ion batteries and olivine $LiFePO_4$ in lithium-ion batteries†

Yujie Zhu, Yunhua Xu, Yihang Liu, Chao Luo and Chunsheng Wang*

Carbon-coated olivine $NaFePO_4$ (C-$NaFePO_4$) spherical particles with a uniform diameter of ~80 nm are obtained by chemical delithiation and subsequent electrochemical sodiation of carbon-coated olivine $LiFePO_4$ (C-$LiFePO_4$), which is synthesized by a solvothermal method. The C-$NaFePO_4$ electrodes are identical (particle size, particle size distribution, surface coating, and active material loading, *etc.*) to C-$LiFePO_4$ except that Li ions in C-$LiFePO_4$ are replaced by Na ions, making them ideal for comparison of thermodynamics and kinetics between C-$NaFePO_4$ cathode in sodium-ion (Na-ion) batteries and C-$LiFePO_4$ in lithium-ion (Li-ion) batteries. In this paper, the equilibrium potentials, reaction resistances, and diffusion coefficient of Na in C-$NaFePO_4$ are systematically investigated by using the galvanostatic intermittent titration technique (GITT), electrochemical impedance spectroscopy (EIS) and cyclic voltammetry (CV), and compared to those of the well-known $LiFePO_4$ cathodes in Li-ion batteries. Due to the lower diffusion coefficient of Na-ion and higher contact and charge transfer resistances in $NaFePO_4$ cathodes, the rate performance of C-$NaFePO_4$ in Na-ion batteries is much worse than that of C-$LiFePO_4$ in Li-ion batteries. However, the cycling stability of C-$NaFePO_4$ is almost comparable to C-$LiFePO_4$ by retaining 90% of its capacity even after 100 charge–discharge cycles at a charge–discharge rate of 0.1 C.

Received 14th September 2012
Accepted 15th November 2012

DOI: 10.1039/c2nr32758a

www.rsc.org/nanoscale

Introduction

Lithium-ion (Li-ion) batteries have been intensively studied for their potential applications in electric vehicles/hybrid electric vehicles over the past decades. Considering the massive application of Li-ion batteries in the future and the limited and unevenly distributed lithium source which is mainly in South America, the cost of lithium will become one of the critical issues for future Li-ion batteries.[1] In contrast to Li-ion batteries, sodium-ion (Na-ion) batteries are potentially cheaper due to the low cost and abundance of sodium in the earth, which makes Na-ion batteries suitable for large scale energy storage devices in which high energy density becomes less critical.[2] Over the past decade, a good deal of academic interest in Na-ion batteries has been focused on the development of cathode materials.[3–10] Layered transition-metal oxides ($NaMO_2$, M = Co, Cr *etc.*) were first proposed to be the cathode materials for Na-ion batteries.[3–8] However, these materials usually show poor cycle life and low thermal stability.[4,5] Also, the reaction mechanisms of these materials are quite complex which usually involve multiple voltage plateaus during the charge–discharge process.[7,8] Among all cathode materials for Na-ion batteries, phosphate polyanion based cathode materials seem to be the most promising candidates due to the relatively high operating potentials and thermal stability.[1] Among phosphate polyanion cathode materials ($NaFePO_4$, $NaVPO_4F$, $Na_3V_2(PO_4)_2F_3$ and Na_2FePO_4F, *etc.*),[1] olivine $NaFePO_4$ has the highest theoretical specific capacity (154 mA h g^{-1}), which makes it an attractive cathode material for Na-ion batteries.

However, so far, only a few reports have been published for electrochemical characterization of olivine $NaFePO_4$ in Na-ion batteries.[11–15] Although olivine $NaFePO_4$ has the same phase structure as olivine $LiFePO_4$, both thermodynamics and reaction kinetics for Na-ion insertion/extraction in $NaFePO_4$ are quite different from the lithiation/delithiation process in $LiFePO_4$.[11–15] It is well-known that lithiation/delithiation in olivine $LiFePO_4$ occurs *via* a two-phase reaction between a Li-deficient phase Li_xFePO_4 ($x \sim 0.05$) and a Li-rich phase $Li_{1-y}FePO_4$ ($y = 0.05$–0.2), while an intermediate $Na_{0.7}FePO_4$ phase was reported during sodiation/desodiation of $NaFePO_4$.[12,13,15] In addition to the different phase transformation thermodynamics, the reaction kinetics (rate performance) and cycling stability of $NaFePO_4$ were also shown to be much worse than $LiFePO_4$.[11,13–15] For example, a specific capacity of 147 mA h g^{-1} for $NaFePO_4$ was reported during the first cycle for the battery operated at 60 °C and C/24 rate, but it quickly

Department of Chemical & Biomolecular Engineering, University of Maryland, College Park, MD 20742, USA. E-mail: cswang@umd.edu; Fax: +1-301-314-9126; Tel: +1-301-405-0352

† Electronic supplementary information (ESI) available. See DOI: 10.1039/c2nr32758a

decreased to 50.6 mA h g^{-1} in the second cycle and the cyclability was limited to 4–5 cycles.[11] Recently, Oh *et al.* reported that $NaFePO_4$ could deliver a specific capacity of 125 mA h g^{-1} over 50 charge–discharge cycles for the battery operated at room temperature and under a very low charge–discharge (C/20) rate.[14] Although the performance of $NaFePO_4$ was improved by Oh *et al.*,[14] it is still not comparable with $LiFePO_4$ in Li-ion batteries. Given olivine $LiFePO_4$ has made a great success in Li-ion batteries,[16–18] a systematic comparison between olivine $LiFePO_4$ in Li-ion batteries and $NaFePO_4$ in Na-ion batteries is critical for further improving the electrochemical performance of $NaFePO_4$ in Na-ion batteries.

To accurately compare the electrochemical properties between $NaFePO_4$ in Na-ion batteries and $LiFePO_4$ in Li-ion batteries, $NaFePO_4$ and $LiFePO_4$ samples should have the same structural properties, such as particle size, particle size distribution, and surface coating, because both thermodynamics and kinetics of $LiFePO_4$ have been shown to be very sensitive to particle size, size distribution and carbon coating.[19–23] For example, minimization of $LiFePO_4$ particle size to 40 nm will decrease the miscibility gap between the lithiated and delithiated phases,[19] increase the equilibrium lithiation potential,[20] and change the phase transformation mechanism fundamentally.[21] The Li-ion diffusion coefficient in $LiFePO_4$ was also shown to be highly dependent on the size of the sample.[22]

Among all synthesis methods, such as hydrothermal,[24] solid-state,[25] sol–gel,[26] and electrospinning,[27] the solvothermal method is able to synthesize uniform nano-$LiFePO_4$ through precise process control and the uniform carbon coating on nano-$LiFePO_4$ can be achieved by polymer coating followed by carbonization. Once the carbon-coated olivine $LiFePO_4$ (C-$LiFePO_4$) is synthesized, carbon-coated olivine $NaFePO_4$ (C-$NaFePO_4$) with identical carbon coating and particle size to C-$LiFePO_4$ can be obtained by chemical (or electrochemical) delithiation of C-$LiFePO_4$ to form carbon-coated olivine $FePO_4$ (C-$FePO_4$), and then followed by electrochemical (or chemical) sodiation of C-$FePO_4$ to form C-$NaFePO_4$.

In this paper, pristine C-$LiFePO_4$ with a uniform diameter of ~80 nm is synthesized by using a solvothermal method followed by carbon coating with sucrose, and C-$FePO_4$ is obtained from chemical delithiation of C-$LiFePO_4$. The C-$NaFePO_4$ with identical particle size, carbon coating and structure to C-$LiFePO_4$ is obtained by electrochemical sodiation of C-$FePO_4$. The electrochemical properties of C-$NaFePO_4$ are investigated and compared to C-$LiFePO_4$. The equilibrium potentials and sodiation/desodiation kinetics of C-$NaFePO_4$ in Na-ion batteries are systematically investigated by using the galvanostatic intermittent titration technique (GITT), electrochemical impedance spectroscopy (EIS) and cyclic voltammetry (CV), and compared to those of C-$LiFePO_4$ in Li-ion batteries.

Experimental section

Materials synthesis

$LiFePO_4$ is prepared from a hydrothermal method. 7.5 mL of 1 M LiOH aqueous solution is first introduced into a mixture of 2.5 mL of 1 M phosphoric acid (H_3PO_4) aqueous solution and 10 mL polyethylene glycol (PEG), which serves as a growth inhibitor. After a milk suspension is formed, 5 mL of 0.5 M $FeSO_4 \cdot 7H_2O$ aqueous solution is slowly introduced into the above mixture under mechanical stirring and continuous argon bubbling. The molar ratio of Li : Fe : P was kept at 3 : 1 : 1. The mixture is then transferred to a Parr autoclave, which is held at 140 °C for 24 h. After naturally cooling to room temperature, the product is collected by centrifugation and washed with acetone and distilled water several times. The final product is dried at 80 °C in a vacuum oven overnight. C-$LiFePO_4$ is prepared by ball milling the as-prepared $LiFePO_4$ with 20 wt% sucrose in acetone for 1 h, and the mixture is then heated to 600 °C for 5 h under argon atmosphere with a heating rate of 2 °C min^{-1}. The percentage of carbon in the C-$LiFePO_4$ is determined by thermogravimetric analysis (TGA), which is about 13% in weight (Fig. S1, ESI†).[28] After chemical delithiation, some carbon is lost due to the strong mechanical agitation. The specific capacity is calculated based on the total mass of $FePO_4$ and residue carbon.

C-$FePO_4$ is obtained from chemical delithiation of C-$LiFePO_4$ by using nitronium tetrafluoroborate (NO_2BF_4) in acetonitrile. 0.1 g C-$LiFePO_4$ is added into a solution of 0.17 g NO_2BF_4 in 10 mL acetonitrile. The mixture is stirred for 24 h at room temperature with continuous argon bubbling, followed by centrifugation and washing with acetonitrile and distilled water several times. The final product is dried at 80 °C in a vacuum oven overnight.

Materials characterizations

The crystal structures of both pristine $LiFePO_4$ and C-$FePO_4$ are characterized by powder X-ray diffraction (XRD) on a D8 Advance with LynxEye and SolX (Bruker AXS, WI, USA) with a Cu-Ka radiation source operated at 40 kV and 40 mA. The morphologies of the pristine $LiFePO_4$ and C-$FePO_4$ samples are characterized by both scanning electron microscopy (SEM) and transmission electron microscopy (TEM) (JEOL JEM 2100F) in the Nanocenter of University of Maryland.

Electrochemical tests

The $FePO_4$ electrode is prepared by the slurry coating method. The material is mixed with 10 wt% carbon black and 8 wt% polyvinylidene fluoride (PVDF) in 1-methyl-2-pyrrolidinone (NMP) solvent to form a viscous paste, which is then mixed for 30 min using a planetary ball milling machine. The obtained slurry is then coated onto aluminium foil and dried in a vacuum oven at 100 °C overnight. Coin cells consisting of an $FePO_4$ cathode, a Na foil anode, Celgard 3501 microporous film separators, and 1.0 M $NaClO_4$ in ethylene carbonate (EC) : dimethyl carbonate (DMC) (1 : 1 by volume) liquid electrolyte are used for electrochemical measurements. For comparison, coin cells consisting of an $FePO_4$ cathode and a Li foil anode are also prepared with 1.0 M $LiPF_6$ in EC:diethyl carbonate (DEC) as the liquid electrolyte.

Galvanostatic charge–discharge is performed by using the *Arbin* test station. Before any electrochemical tests, the Na/$FePO_4$ cell is discharged to 2.0 V and the Li/$FePO_4$ cell is discharged to 2.5 V with a constant current of 0.01 C to form

$NaFePO_4$ and $LiFePO_4$ in the cells, respectively. All C-rates used in this study are calculated based on the theoretical capacity of 154 mA h g^{-1} for $NaFePO_4$ and 170 mA h g^{-1} for $LiFePO_4$. The cells are cycled between 2.0 and 4.0 V for $NaFePO_4$ cells, and between 2.5 and 4.0 V for $LiFePO_4$ cells at different current rates. After the cell reaches the cut-off voltages, it is relaxed for 5 min before subsequent charge or discharge. Before the galvanostatic charge–discharge tests, the cells are pre-cycled 5 times at a current of 0.1 C. The equilibrium (open-circuit) potential of the cells is obtained by a galvanostatic intermittent titration technique (GITT), which consists of a series of current pulses at 0.025 C (for the $NaFePO_4$ cell) or 0.05 C (for the $LiFePO_4$ cell) for 1 h, followed by a 15 h relaxation process. The open-circuit-voltage (OCV) at the end of relaxation is considered to be the thermodynamically equilibrium potential.

Cyclic voltammetry (CV) tests with voltages ranging from 2.0 V to 3.8 V for the $NaFePO_4$ cell and 2.5 V to 4.0 V for the $LiFePO_4$ cell are performed under various scan rates. Before each CV test, the $NaFePO_4$ cell is galvanostatically discharged to 2.0 V (2.5 V for the $LiFePO_4$ cell) at a current of 0.05 C. Electrochemical impedance spectroscopy (EIS) tests with frequency ranging from 10^6 Hz to 10^{-3} Hz are performed on both $NaFePO_4$ and $LiFePO_4$ cells. The loading amounts of active materials for EIS tests are 1.7 mg for the $NaFePO_4$ cell and 1.4 mg for the $LiFePO_4$ cell, respectively. Before the EIS tests, the $NaFePO_4$ cell is charged–discharged for 20 cycles and then discharged to 2 V (2.5 V for the $LiFePO_4$ cell) with a current of 0.05 C, followed by a 2 h relaxation. Both CV and EIS tests are recorded by using Solatron 1260/1287 Electrochemical Interface (Solatron Metrology, UK).

Results and discussion

Materials synthesis and characterizations

Scheme 1 shows the synthesis process of materials. C-$LiFePO_4$ is synthesized from a solvothermal method followed by carbon coating with sucrose (Scheme 1a). Then, C-$LiFePO_4$ is chemically delithiated to form C-$FePO_4$ (Scheme 1b). Finally, chemically delithiated C-$FePO_4$ is used in both Li-ion batteries and Na-ion batteries to electrochemically form C-$LiFePO_4$ and C-$NaFePO_4$ (Scheme 1c and d), which guarantees the identical properties between $NaFePO_4$ and $LiFePO_4$ electrodes. Fig. 1a shows the X-ray diffraction (XRD) patterns for pristine $LiFePO_4$ and C-$FePO_4$ obtained from chemical delithiation of C-$LiFePO_4$. Both XRD patterns are indexed in the orthorhombic (*pnma*) crystallographic system and in good agreement with the reported results in the literature.[29] Both XRD patterns show that there are no detectable impurities in the samples, especially no residue Li is detected in the C-$FePO_4$ sample which ensures that the one-dimensional (1D) channels for Li-ion insertion/extraction are not blocked. Fig. 1b and c show the SEM and TEM images for the pristine $LiFePO_4$. As shown in Fig. 1b and c, pristine $LiFePO_4$ has a nearly spherical shape with a uniform diameter of ~80 nm, which makes this sample well suitable for fundamental study since it minimizes the effect of particle size distribution. Fig. 1d shows the high resolution TEM (HRTEM) image of one C-$FePO_4$ particle, on the surface of which a layer (<10 nm) of carbon is clearly observed.

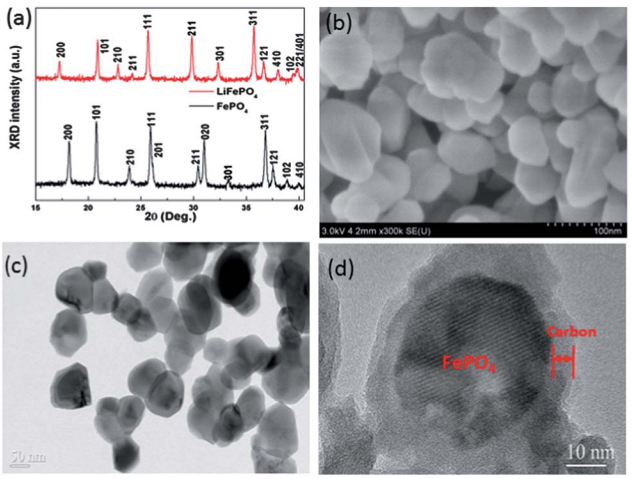

Fig. 1 (a) XRD patterns of pristine $LiFePO_4$ and C-$FePO_4$ obtained from chemical delithiation of C-$LiFePO_4$, (b) SEM image of pristine $LiFePO_4$, (c) TEM image of pristine $LiFePO_4$ and (d) HRTEM image of the C-$FePO_4$ sample obtained from chemical delithiation C-$LiFePO_4$.

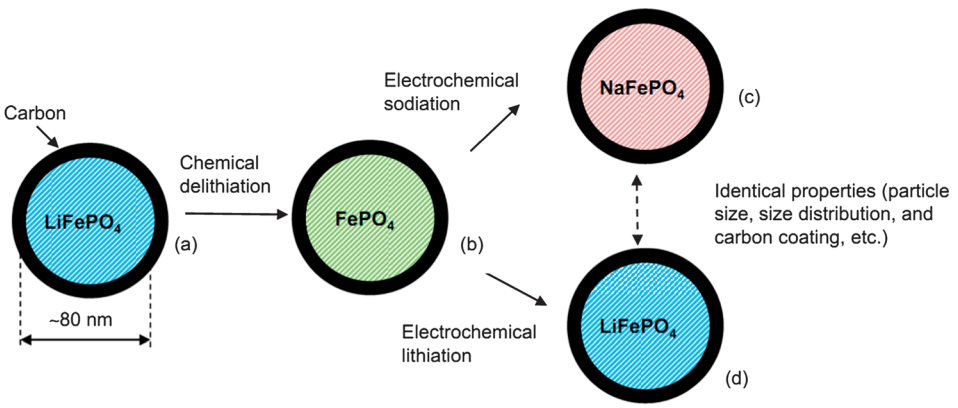

Scheme 1 Illustration of the synthesis process for C-$LiFePO_4$ and C-$NaFePO_4$ with identical properties.

Thermodynamic properties of $NaFePO_4$ and $LiFePO_4$

Fig. 2a and b show the open-circuit-voltage (OCV) for lithiation/delithiation in C-$LiFePO_4$ and sodiation/desodiation in C-$NaFePO_4$, respectively. The OCVs of C-$LiFePO_4$ show two very flat potential plateaus around 3.40 V (*vs.* Li/Li^+) during lithiation and 3.43 V (*vs.* Li/Li^+) during delithiation (Fig. 2a). The potential hysteresis between lithiation and delithiation is around 30 mV. For C-$NaFePO_4$, one potential plateau at 2.86 V *vs.* Na/Na^+ for sodiation is observed, which is 540 mV lower than the OCV of phase transformation from $FePO_4$ to $LiFePO_4$ in Li-ion batteries. Interestingly, two distinct potential plateaus, which are 2.88 V (*vs.* Na/Na^+) and 3.02 V (*vs.* Na/Na^+), are obtained for Na-ion extraction from C-$NaFePO_4$ as shown by the discontinuity around $Na_{0.7}FePO_4$ in the potential–composition curve (Fig. 2b). Moreau *et al.* also reported one potential plateau during Na-ion insertion and two potential plateaus for Na-ion extraction from $NaFePO_4$ and the two potential plateaus were corresponding to the formation of the intermediate $Na_{0.7}FePO_4$ phase during phase transition from $NaFePO_4$ to $FePO_4$.[12] The potential hysteresis between Na-ion insertion and extraction at the same Na content is around 140 mV, which is more than 4 times larger than that of $LiFePO_4$ in Li-ion batteries. The observed potential hysteresis is in analogous to the pressure hysteresis reported in metal hydride materials, which is usually related to the transformation strains and attributed to the plastic deformation during phase transition.[30] The hysteresis energy loss was thought to be the energy spent to create dislocations in the materials during phase transition.[30] Given the volume difference between $NaFePO_4$ and $FePO_4$ is larger than that between $LiFePO_4$ and $FePO_4$, the potential hysteresis of $NaFePO_4$ is also larger than that of $LiFePO_4$. Other reasons, such as the sequential particle-by-particle charge–discharge mechanism proposed by Dreyer *et al.*, may also account for the observed potential hysteresis difference between $LiFePO_4$ and $NaFePO_4$.[31]

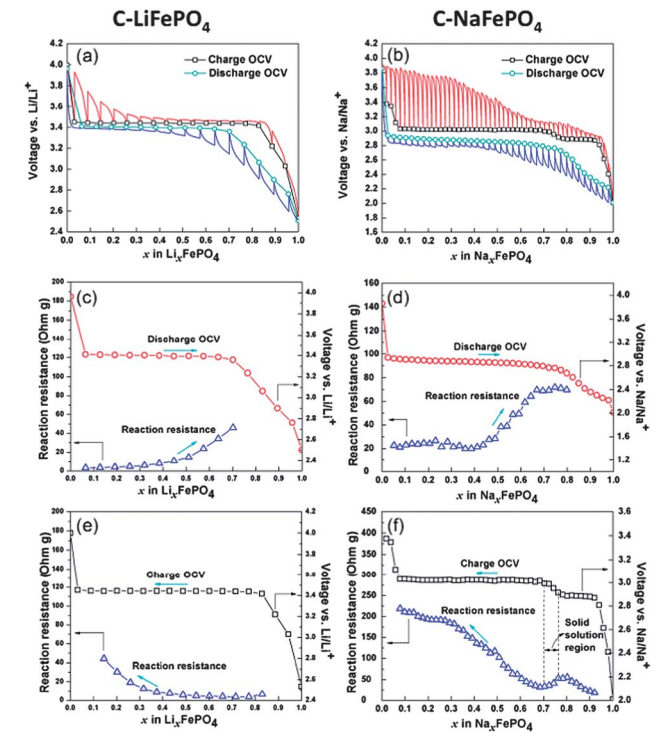

Fig. 2 (a) Equilibrium (open-circuit)–voltage (symbols) and transient voltage profiles (solid lines) *versus* Li composition in C-Li_xFePO_4 for Li extraction/insertion in C-$LiFePO_4$ obtained from GITT, (b) equilibrium (open-circuit)–voltage (symbols) and transient voltage profiles (solid lines) *versus* Na composition in C-Na_xFePO_4 for Na extraction/insertion in C-$NaFePO_4$ obtained from GITT, (c) reaction resistance for Li insertion into C-$FePO_4$, (d) reaction resistance for Na insertion into C-$FePO_4$, (e) reaction resistance for Li extraction from C-$LiFePO_4$ and (f) reaction resistance for Na extraction from C-$NaFePO_4$. Note: both Li and Na compositions for charge–discharge are obtained by normalizing the charge–discharge capacity.

Kinetics of $NaFePO_4$ and $LiFePO_4$

The reaction resistances of C-$LiFePO_4$ and C-$NaFePO_4$, defined as the ratio of overpotential to the pulse current density, are used to compare the reaction kinetics of C-$NaFePO_4$ and C-$LiFePO_4$. Fig. 2c–f show reaction resistances of C-$LiFePO_4$ and C-$NaFePO_4$ in phase transformation regions. During Li-ion insertion and extraction, the reaction resistances follow a similar tendency, which gradually increase with the degree of phase transition and reach a maximum value of 45 Ohm g at the end of potential plateaus (Fig. 2c and e).

For Na-ion insertion into $FePO_4$ (Fig. 2d), the reaction resistance maintains at 20 Ohm g during initial Na-ion insertion, but begins to increase after the Na content reaches 0.45, and levels off at 70 Ohm g after the Na content reaches 0.7. The reaction resistance during Na-ion extraction from C-$NaFePO_4$ (Fig. 2f) shows a continuous increase at each potential plateau but a steep decrease at the beginning of the second phase transformation at 3.02 V. Na-ion extraction shows a higher reaction resistance than Na-ion insertion, and the exact reason is not clear so far. From the reaction resistance and equilibrium potential curves (Fig. 2f), the solubility of the $Na_{0.7}FePO_4$ intermediate phase is estimated to be around 0.06 ($Na_{0.7\sim0.76}FePO_4$). The increase in reaction resistance during the phase change from $NaFePO_4$ to $Na_{0.7}FePO_4$ is similar to the change of reaction resistance from $FePO_4$ to $NaFePO_4$ during Na-ion insertion. However, the reaction resistance in the second voltage plateau from $Na_{0.7}FePO_4$ to $FePO_4$ increases from 20 Ohm g to 200 Ohm g. This can be partially explained by the much larger volume difference between $Na_{0.7}FePO_4$ and $FePO_4$ compared to that from $NaFePO_4$ to $Na_{0.7}FePO_4$. It has been shown that the unit volume difference between $Na_{0.7}FePO_4$ and $FePO_4$ is 13.48%, which is more than 3 times larger than that from $NaFePO_4$ to $Na_{0.7}FePO_4$ (3.46%).[15] Other reasons, such as the surface chemical potential barrier and electronic migration,[32,33] may also account for the observed reaction resistance difference. A similar reaction resistance jump was also reported by us in graphite anodes of a Li-ion cell in which lithiated graphite experienced three successive stage transformations during Li extraction.[34] Recently, Gu *et al.* reported that $LiFePO_4$ actually experienced a stage transformation process during lithiation/delithiation which is analogous to the staging phenomenon observed in some layered intercalation compounds.[35] The two successive stage phase transformations for Na-ion extraction from $NaFePO_4$ rather than single stage

transformation in $LiFePO_4$ may be attributed to a much higher strain during phase transformation from $NaFePO_4$ to $FePO_4$, which is caused by the large ionic radius of Na-ion.

From the transient voltage responses during the GITT tests, we can calculate the chemical diffusion coefficient for both Na (D_{Na}) and Li (D_{Li}) in $FePO_4$ according to eqn (1) (ref. 36 and 37)

$$D = \frac{4}{\pi}\left(\frac{IV_m}{FS}\right)^2 \left[\left(dE/dx/dE/dt^{0.5}\right)\right]^2 \quad (1)$$

where I is the applied constant current density (for $LiFePO_4$ I = 8.5 mA g^{-1}, for $NaFePO_4$ I = 3.85 mA g^{-1}), V_m is the molar volume of phosphate (44.11 cm^3 mol^{-1}),[37] F is the Faraday constant (96 486 C mol^{-1}), S is the contact area between electrolyte and active materials which is taken as 1/3 of the total Brunauer–Emmett–Teller (BET) surface area (S_{BET} = 249616 cm^2 g^{-1}) since, similar to the $LiFePO_4$ system, Na-ion insertion/extraction in olivine $NaFePO_4$ is expected to only happen at the channels running along the [010] direction, dE/dx is the slope of the coulometric titration curve at composition x and $dE/dt^{0.5}$ can be obtained from the plot of the transient voltage *versus* the square root of time during constant current pulse.

Since eqn (1) was derived by assuming ion diffusion in one-dimensional solid solution electrode materials,[36] it is not valid at the phase transition regions,[38] in which the value of dE/dx should be zero according to the Gibbs phase rule. So we only use eqn (1) to calculate the ion diffusion coefficient near the end of discharge, which is corresponding to a solid solution material with a composition of $Na_{0.9}FePO_4$ or $Li_{0.9}FePO_4$.

Fig. 3 shows the plot of transient voltage *versus* the square root of the time for $Na_{0.9}FePO_4$ and $Li_{0.9}FeO_4$, and the linear fitting of the first 200 s is also shown in the plot. Plugging the slope of the linear fitting into eqn (1), we can get the diffusion coefficient of lithium D_{Li} and sodium D_{Na}, which are $D_{Li} = 6.77 \times 10^{-16}$ cm^2 s^{-1} and $D_{Na} = 8.63 \times 10^{-17}$ cm^2 s^{-1}, respectively.

The reaction resistances in Fig. 2c–f reflect the total resistances of electrolyte, contact resistance of particle-to-particle and particle-to-current collector, charge transfer, and ion diffusion in host materials. To separate these resistances, electrochemical impedance spectroscopy (EIS) in the frequency ranging from 10^6 Hz to 10^{-3} Hz at a 10 mV amplitude is applied to C-$NaFePO_4$ and C-$LiFePO_4$ cells at fully discharged states after 20 charge–discharge cycles. Fig. 4 shows the Nyquist plots for C-$NaFePO_4$ and C-$LiFePO_4$ cells. The Nyquist plots consist of two semicircles at high and middle frequency and a straight line at low frequency, although the high and middle frequency semicircles for C-$LiFePO_4$ seem to be overlapped into one depressed semicircle. For the olivine cathode, the high frequency semicircle is attributed to either the contact impedance of particle-to-particle and particle-to-current collector or the impedance of the passivating layer,[39–43] the middle frequency semicircle is usually due to the charge transfer resistance,[41–43] and the low frequency line is the characteristic of ion diffusion inside the host materials.

To further understand the different reaction kinetics between $NaFePO_4$ and $LiFePO_4$, the impedance data are fitted with the equivalent circuit shown in the inset of Fig. 4. The resistor R_s corresponds to the electrolyte resistance. The

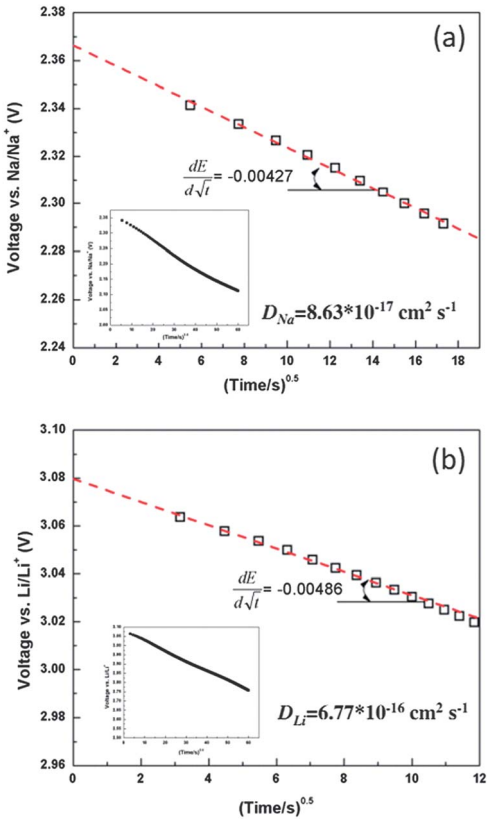

Fig. 3 Plot of transient voltage *versus* the square root of the time during the galvanostatic pulse for (a) $Na_{0.9}FePO_4$ and (b) $Li_{0.9}FePO_4$. The red dashed line is the linear fitting of the first 200 s, and the slope of the linear fitting is presented in the plot. The inset figure is the same plot in a full scale. Note: the calculated diffusion coefficient is also presented in the plot.

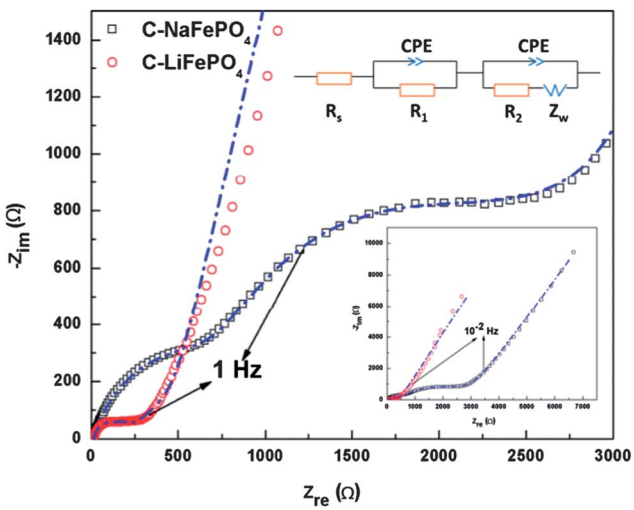

Fig. 4 Nyquist plots for $NaFePO_4$ and $LiFePO_4$ cells obtained by electrochemical impedance spectroscopy (EIS) tests at fully discharged states after 20 charge–discharge cycles. The blue dashed lines are the fitting curve by using the equivalent circuit which is shown as the inset and consists of a resistor (R_s), a resistor (R_1) paralleled with a constant phase element (CPE), and a CPE parallel with a resistor (R_2) which is connected with a Warburg element (Z_w) in series. Note: the inseted figure is the Nyquist plot in a full scale.

Table 1 Electrode resistances for C-$LiFePO_4$ and C-$NaFePO_4$ obtained from equivalent circuit fitting of EIS results

	C-$LiFePO_4$	C-$NaFePO_4$
R_s (Ω)	14.74	8.915
R_1 (Ω)	105.4	790.2
R_2 (Ω)	95.32	1204

resistors R_1 and R_2 paralleled with the constant phase element (CPE) account for the contact impedance and charge transfer impedance, respectively. The ion diffusion in the host material is described with the Warburg element (Z_w). As shown in Fig. 4, the simulated data from the equivalent circuit well fit the impedance data for both C-$LiFePO_4$ and C-$NaFePO_4$. The values for the different resistances obtained from fitting are listed in Table 1.

As shown in Table 1, although the electrolyte resistance is almost the same for C-$LiFePO_4$ and C-$NaFePO_4$ cells, both the contact and charge transfer impedances of C-$NaFePO_4$ are much higher than those of C-$LiFePO_4$. The high contact resistance of C-$NaFePO_4$ may attribute to the large volume change of C-$NaFePO_4$ during charge–discharge and the large charge transfer resistance of C-$NaFePO_4$ cell may be due to the relatively larger size of Na-ion. The total impedances including contact resistance and charge transfer resistance in the C-$NaFePO_4$ cell are almost 10 times larger than those in the C-$LiFePO_4$ cell, which is consistent with the reaction resistance difference in Fig. 2.

From the EIS tests, the ion diffusion coefficient can be calculated by using eqn (2) (ref. 37)

$$D = \frac{1}{2}\left[\left(\frac{V_m}{AF\delta}\right)\left(\frac{dE}{dx}\right)\right]^2 \quad (2)$$

where δ is the slope of the Warburg straight line ($\Omega\ s^{-1}$), A (cm^2) is the effective contact area between the electrolyte and sample which can be obtained by multiplying S in eqn (1) by the loading amount of active materials, and other symbols have the same meaning as they have in eqn (1).

Fig. 5 shows the plot of the imaginary resistance *versus* the inverse square root of angular frequency ranging from 10^{-2} Hz to 10^{-3} Hz. As shown in Fig. 5, a linear behaviour can be obtained for both C-$NaFePO_4$ and C-$LiFePO_4$. Plugging the slope of the linear fitting into eqn (2), we can get the diffusion coefficient for lithium and sodium, which are $D_{Li} = 1.80 \times 10^{-15}\ cm^2\ s^{-1}$ and $D_{Na} = 8.70 \times 10^{-17}\ cm^2\ s^{-1}$, respectively, and close to the values obtained from the GITT tests (Fig. 3).

From both the GITT and EIS tests, the chemical diffusion coefficient of Na-ion is shown to be of the order of $\sim 10^{-17}\ cm^2\ s^{-1}$. The calculated chemical diffusion coefficients for Na-ion in Na_xFePO_4 are 1–2 orders lower than those for Li-ion in the Li_xFePO_4 system. This result is consistent with the theoretical calculation, in which Na and vacancy diffusion barriers in the Na_xFePO_4 system are predicted to be higher than those for Li in the Li_xFePO_4 system.[44] The lower diffusion constant of Na in Na_xFePO_4 compared to that of Li in Li_xFePO_4 can be explained by the rigid oxygen framework, which limits the accommodation of Na with a larger ionic radius.

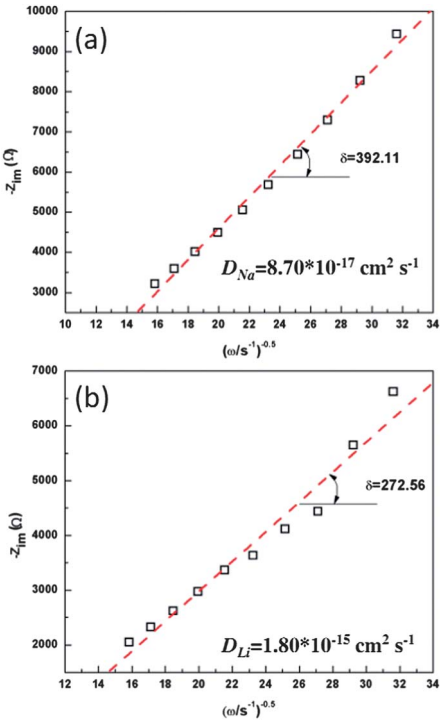

Fig. 5 The plot of the imaginary resistance *versus* the inverse square root of angular frequency for (a) C-$NaFePO_4$ and (b) C-$LiFePO_4$. The frequency values range from 10^{-2} Hz to 10^{-3} Hz. The red dashed line corresponds to the linear fitting with the slope marked out.

The different reaction kinetics between C-$NaFePO_4$ and C-$LiFePO_4$ are also investigated by cyclic voltammetry (CV). Fig. 6a and b show the CV results for C-$NaFePO_4$ and C-$LiFePO_4$ cells under different scan rates. The CV scan of C-$LiFePO_4$ shows one distinct anodic peak and one cathodic peak (Fig. 6a). However, for C-$NaFePO_4$, two well defined current peaks are found for the anodic process and only one current peak is observed for the cathodic scan (Fig. 6b), which is consistent with the results measured from GITT. The value of the current peak for C-$LiFePO_4$ is more than 10 times higher than that for C-$NaFePO_4$ at the same scan rate, which demonstrates the poor reaction kinetics of Na-ion insertion/extraction in $NaFePO_4$ and is consistent with the results obtained from GITT and EIS tests.

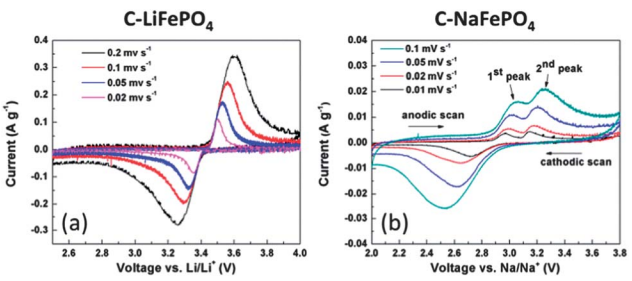

Fig. 6 Cyclic voltammetry (CV) tests for (a) C-$LiFePO_4$ in the Li-ion cell and (b) C-$NaFePO_4$ in the Na-ion cell under different scan rates.

Electrochemical performance of $NaFePO_4$ and $LiFePO_4$

Electrochemical performances of C-$NaFePO_4$ and C-$LiFePO_4$ are compared in Fig. 7. Fig. 7a shows the cycling stability of the C-$NaFePO_4$ cell at a constant current of 0.1 C (15.4 mA g^{-1}). The C-$NaFePO_4$ cell can deliver approximately a reversible capacity of 100 mA h g^{-1} with the coulombic efficiency higher than 94%. 100 mA h g^{-1} is calculated based on total mass of $FePO_4$ and the coated carbon in the electrode. The C-$NaFePO_4$ cell retains 90% of capacity even after 100 charge–discharge cycles. The cycling stability of the C-$NaFePO_4$ cell is comparable with that of the C-$LiFePO_4$ cell (Fig. 7e). The exceptional cycling stability of C-$NaFePO_4$ is consistent with the theoretical calculations,[12] which suggested that olivine $NaFePO_4$ has strong poly-anion P–O bonds, making it not be transformed into an electrochemically inactive maricite phase during cycling. Fig. 7b shows the voltage profiles of the C-$NaFePO_4$ cell at different charge–discharge cycles under a current of 0.1 C (15.4 mA g^{-1}) at room temperature. Similar to the GITT result, two voltage plateaus are present during charge and only one for discharge. As shown in the charge–discharge curves (Fig. 7b), the voltage plateaus in the C-$NaFePO_4$ cell are steeper compared with the very flat voltage plateaus in the C-$LiFePO_4$ cell (Fig. 7f). Since the equilibrium potentials for Na-ion extraction/insertion in the C-$NaFePO_4$ cell are also flat (Fig. 2b), the sloped voltage profile in the C-$NaFePO_4$ cell at a 0.1 C rate is attributed to high polarization induced by slow reaction kinetics during Na-ion insertion/extraction in C-$NaFePO_4$.

The rate capability of the C-$NaFePO_4$ cell at six different C-rates is shown in Fig. 7c and the corresponding charge–discharge curves are shown in Fig. 7d. All C-rates are calculated based on the theoretical capacity of $NaFePO_4$ (154 mA h g^{-1}). As shown in Fig. 7c, the C-$NaFePO_4$ cell can provide stable discharge capacities of 120, 100, 84, 60, 40 and 23 mA h g^{-1} at 0.05 C, 0.1 C, 0.2 C, 0.5 C, 1 C and 2 C, respectively. The discharge capacity of C-$FePO_4$ in the C-$NaFePO_4$ cell at 2 C is only 23% of its capacity at 0.1 C, while the same C-$FePO_4$ in the C-$LiFePO_4$ cell can provide 70% of its capacity at 0.1 C (Fig. 7f). As shown in Fig. 7d, the large overpotentials (>1 V) presented at the discharge current of 2 C imply the poor kinetics of C-$NaFePO_4$ cells at high C-rates.

Since both C-$NaFePO_4$ and C-$LiFePO_4$ are formed by electrochemical ion insertion into the same C-$FePO_4$, the worse rate capability of the C-$NaFePO_4$ cell (Fig. 7c) than that of the C-$LiFePO_4$ cell (Fig. 7f) can be mainly attributed to the low chemical diffusion coefficient of Na-ion in $NaFePO_4$ (Fig. 3 and 5) and large contact and charge transfer resistances (Table 1). Moreover, the 17% volume change upon phase transition from C-$FePO_4$ to C-$NaFePO_4$ may also contribute to the observed poor rate performance of C-$NaFePO_4$. This 17% volume change is even larger than that in $LiMnPO_4$ (10%), which often shows poor rate capability due to the large lattice misfit between $MnPO_4$ and $LiMnPO_4$.[45] Similar to $LiMnPO_4$,[45] this large misfit induced strain in $NaFePO_4$ can cause dislocations/cracks during charge–discharge cycles, increasing the contact resistance and also hindering the phase transition kinetics in C-$NaFePO_4$ as demonstrated by large polarization and high reaction resistance in Fig. 2, especially during Na-ion extraction.

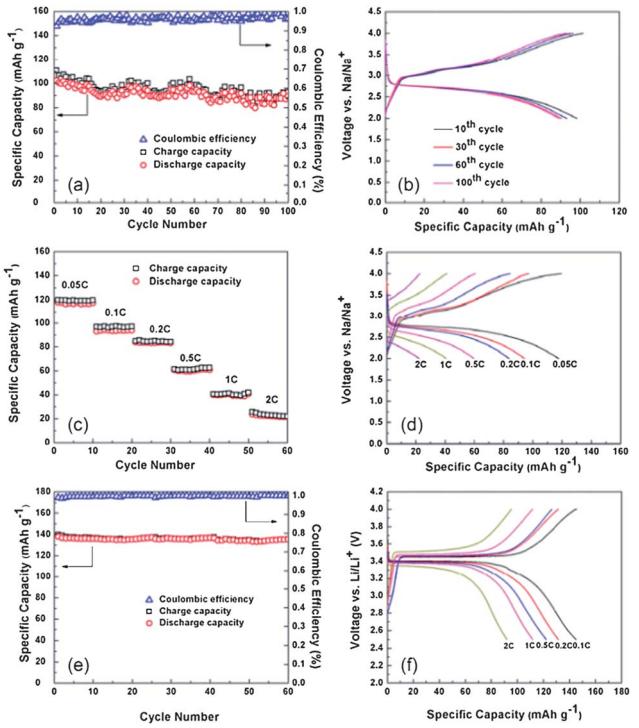

Fig. 7 Electrochemical tests for C-$LiFePO_4$ and C-$NaFePO_4$ cells. (a) Cycling stability test of the C-$NaFePO_4$ cell at a 0.1 C (15.4 mA g^{-1}) charge–discharge current, (b) voltage profiles of the C-$NaFePO_4$ cell at different charge–discharge cycles under a 0.1 C (15.4 mA g^{-1}) charge–discharge current, (c) rate capability test of the C-$NaFePO_4$ cell at different charge-discharge C-rates, (d) voltage profiles at different charge–discharge C-rates for the C-$NaFePO_4$ cell, (e) cycle stability test for the C-$LiFePO_4$ cell at a current of 0.1 C (17 mA g^{-1}) and (f) rate capability test for the C-$LiFePO_4$ cell.

Conclusions

In summary, both thermodynamics and reaction kinetics of Na-ion insertion/extraction in carbon-coated olivine $NaFePO_4$ in Na-ion batteries are systematically investigated and compared to those of carbon-coated olivine $LiFePO_4$ in Li-ion batteries. Thermodynamics analysis of C-$NaFePO_4$ cells using GITT reveals two potential plateaus during Na-ion extraction from C-$NaFePO_4$ but only one potential plateau for Na-ion insertion into C-$FePO_4$, which is different from C-$LiFePO_4$. Electrochemical tests show that C-$NaFePO_4$ can maintain 90% of initial capacity even after 100 full charge–discharge cycles in Na-ion batteries. Although the cyclability of C-$NaFePO_4$ is comparable with that of C-$LiFePO_4$ in Li-ion cells, the rate performance of C-$NaFePO_4$ cells is shown to be much worse than those of C-$LiFePO_4$ cells with the same C-$FePO_4$. Detailed kinetic studies using GITT, EIS and CV reveal that the slow Na-ion insertion/extraction kinetics are attributed to (1) 1–2 orders of magnitude lower diffusion coefficient of Na-ion in Na_xFePO_4 than that of Li-ion in Li_xFePO_4, (2) 10 times higher contact and charge transfer resistances in the C-$NaFePO_4$ cell than those in the C-$LiFePO_4$ cell, and (3) a more than two times larger volume change between C-$FePO_4$ and C-$NaFePO_4$ than that in C-$FePO_4$ and C-$LiFePO_4$.

Acknowledgements

Financial support by the National Science Foundation under Contract no. CBET0933228 (Dr. Maria Burka, Program Director) is gratefully acknowledged. The authors also acknowledge the technical support from the University of Maryland NanoCenter.

Notes and references

1 V. Palomares, P. Serras, I. Villaluenga, K. B. Hueso, J. Carretero-Gonzalez and T. Rojo, *Energy Environ. Sci.*, 2012, **5**, 5884–5901.
2 S.-W. Kim, D.-H. Seo, X. Ma, G. Ceder and K. Kang, *Adv. Energy Mater.*, 2012, **2**, 710–721.
3 M. M. Doeff, Y. Ma, S. J. Visco and L. C. De Jonghe, *J. Electrochem. Soc.*, 1993, **140**, 169–170.
4 S. Komaba, T. Nakayama, A. Ogata, T. Shimizu, C. Takei, S. Takada, A. Hokura and I. Nakai, *ECS Trans.*, 2009, **16**, 43–55.
5 S. Komaba, C. Takei, T. Nakayama, A. Ogata and N. Yabuuchi, *Electrochem. Commun.*, 2010, **12**, 355–358.
6 X. Xia and J. R. Dahn, *Electrochem. Solid-State Lett.*, 2012, **15**, A1–A4.
7 R. Berthelot, D. Carlier and C. Delmas, *Nat. Mater.*, 2010, **10**, 74–80.
8 F. Sauvage, L. Laffont, J.-M. Tarascon and E. Baudrin, *Inorg. Chem.*, 2007, **46**, 3289–3294.
9 B. L. Ellis, W. R. M. Makahnouk, Y. Makimura, K. Toghill and L. F. Nazar, *Nat. Mater.*, 2007, **6**, 749–753.
10 F. Sauvage, E. Quarez, J.-M. Tarascon and E. Baudrin, *Solid State Sci.*, 2006, **8**, 1215–1221.
11 K. Zaghib, J. Trottier, P. Hovington, F. Brochu, A. Guerfi, A. Mauger and C. M. Julier, *J. Power Sources*, 2011, **196**, 9612–9617.
12 P. Moreau, D. Guyomard, J. Gaubicher and F. Boucher, *Chem. Mater.*, 2010, **22**, 4126–4128.
13 K. T. Lee, T. N. Ramesh, F. Nan, G. Botton and L. F. Nazar, *Chem. Mater.*, 2011, **23**, 3593–3600.
14 S.-M. Oh, S.-T. Myung, J. Hassoun, B. Scrosati and Y.-K. Sun, *Electrochem. Commun.*, 2012, **22**, 149–152.
15 M. Casas-Cabanas, V. Roddatis, D. Saurel, P. Kubiak, J. Carretero-Gonzalez, V. Palomares, P. Serras and T. Rojo, *J. Mater. Chem.*, 2012, **22**, 17421–17423.
16 A. K. Padhi, K. S. Nanjundaswamy and J. B. Goodenough, *J. Electrochem. Soc.*, 1997, **144**, 1188–1194.
17 S.-Y. Chung, J. T. Bloking and Y.-M. Chiang, *Nat. Mater.*, 2002, **1**, 123–128.
18 B. Kang and G. Ceder, *Nature*, 2009, **458**, 190–193.
19 N. Meethong, H.-Y. Huang, W. Craig Carter and Y. M. Chiang, *Electrochem. Solid-State Lett.*, 2007, **10**, A134–A138.
20 K. T. Lee, W. H. Kan and L. F. Nazar, *J. Am. Chem. Soc.*, 2009, **131**, 6044–6045.
21 P. Gibot, M. C. Cabanas, L. Laffont, S. Levasseur, P. Carlach, S. P. Hamelet, J.-M. Tarascon and C. Masquelier, *Nat. Mater.*, 2008, **7**, 741–744.
22 R. Malik, D. Burch, M. Bazant and G. Ceder, *Nano Lett.*, 2010, **10**, 4123–4127.
23 Y. Zhu and C. Wang, *J. Power Sources*, 2011, **10**, 1442–1448.
24 K. Dokko, S. Koizumi, H. Nakano and K. Kanamura, *J. Mater. Chem.*, 2007, **17**, 4803–4810.
25 H.-C. Kang, D.-K. Jun, B. Jin, E. M. Jin, K.-H. Park, H.-B. Gu and K.-W. Kim, *J. Power Sources*, 2008, **15**, 340–346.
26 Y. Q. Hu, M. M. Doeff, R. Kostecki and R. Finones, *J. Electrochem. Soc.*, 2004, **151**, A1279–A1285.
27 C. B. Zhu, Y. Yu, L. Gu, K. Weichert and J. Maier, *Angew. Chem., Int. Ed.*, 2011, **50**, 6278–6282.
28 C. Nan, J. Lu, C. Chen, Q. Peng and Y. Li, *J. Mater. Chem.*, 2011, **21**, 9994–9996.
29 C. V. Ramana, A. Mauger, F. Gendron, C. M. Julien and K. Zaghib, *J. Power Sources*, 2009, **187**, 555–564.
30 R. Balasubramaniam, *J. Alloys Compd.*, 1997, **253**, 203–206.
31 W. Dreyer, J. Jamnik, C. Guhlke, R. Huth, J. Moskon and M. Gaberscek, *Nat. Mater.*, 2010, **9**, 448–453.
32 L. Wang, F. Zhou and G. Ceder, *Electrochem. Solid-State Lett.*, 2008, **11**, A94–A96.
33 S. P. Ong, V. L. Chevier and G. Ceder, *Phys. Rev. B: Condens. Matter Mater. Phys.*, 2011, **83**, 0755112.
34 C. Wang, I. Kakwan, A. J. Appleby and F. E. Little, *J. Electroanal. Chem.*, 2000, **489**, 55–67.
35 L. Gu, C. Zhu, H. Li, Y. Yu, C. Li, S. Tsukimoto, J. Maier and Y. Ikuhara, *J. Am. Chem. Soc.*, 2011, **133**, 4661–4663.
36 C. J. Wen, B. A. Boukamp, R. A. Huggins and W. Weppner, *J. Electrochem. Soc.*, 1979, **126**, 2258–2266.
37 P. P. Prosini, M. Lisi, D. Zane and M. Pasquali, *Solid State Ionics*, 2002, **148**, 45–51.
38 Y. Zhu and C. Wang, *J. Phys. Chem. C*, 2010, **114**, 2830–2841.
39 M. Gaberscek, R. Dominko and J. Jamnik, *J. Power Sources*, 2007, **174**, 944–948.
40 J.-M. Atebamba, J. Moskon, S. Pejovnik and M. Gabersceka, *J. Electrochem. Soc.*, 2010, **157**, A1218–A1228.
41 H. C. Shin, W. I. Cho and H. Jang, *Electrochim. Acta*, 2006, **52**, 1475–1476.
42 J. P. Schmidt, T. Chrobak, M. Ender, J. Illig, D. Klotz and E. Ivers-Tiffee, *J. Power Sources*, 2011, **196**, 5342–5348.
43 J. Illig, M. Ender, T. Chrobak, J. P. Schmidt, D. Klotz and E. Ivers-Tiffee, *J. Electrochem. Soc.*, 2012, **159**, A952–A960.
44 S. P. Ong, V. L. Chevrier, G. Hautier, A. Jain, C. Moore, S. Kim, X. Ma and G. Ceder, *Energy Environ. Sci.*, 2011, **4**, 3680–3688.
45 N. Meetong, H. Huang, S. Speakman, W. C. Carter and Y. M. Chiang, *Adv. Funct. Mater.*, 2007, **17**, 1115–1123.